Current status of mid-infrared quantum and interband cascade lasers for clinical breath analysis

Terence H. Risby
Johns Hopkins University
Bloomberg School of Public Health
Department of Environmental Health Sciences
615 North Wolfe Street
Baltimore, Maryland 21205

Frank K. Tittel
Rice University
Department of Electrical and Computer Engineering, MS366
6100 Main Street
Houston, Texas 77005

Abstract. State-of-the-art quantum- and interband-cascade-based chemical sensors may be effective new tools for the identification and quantification of trace gases in human breath for clinical uses. Increased or decreased concentrations of these molecules are associated with the pathogenesis of a large number of diseases. Current technologies enable breath analyses to be performed on a single breath and the results are available in real time. Critical parameters including sensor sensitivity, selectivity, real-time monitoring capability, robustness, cost, size, and weight determine the progress ~~that~~ made toward the development and availability of commercial diagnostic material. [DOI: 10.1117/1.3498768]

Subject terms: mid-infrared semiconductor-laser-based chemical sensor; real-time breath analysis; breath sampling; quantum cascade lasers; interband cascade lasers; single-frequency, tunable external cavity quantum cascade/interband lasers.

Paper 100329SSR received Apr. 14, 2010; revised manuscript received Jun. 4, 2010; accepted for publication Jun. 14, 2010; published online Nov. 00, 2010.

1 Introduction

This paper reviews the current status of mid-IR semiconductor lasers for clinical breath analysis and attempts to suggest future directions. Clinical breath analysis remains in its infancy, despite the fact that its potential has been recognized since antiquity. Most of this limitation is due to the lack of availability of sensors designed specifically for breath analysis with the result that most of the published breath analyses are based on the use of standard analytical chemistry instrumentation. The wider availability of real-time, portable laser-based breath monitors would be a breakthrough to clinical practice since interlaboratory data could be compared and contrasted and also large populations of normal and diseased humans could be studied. Based on current knowledge, limits of quantification in the range of 1 ppb are required with instrumental response times of 10 Hz. Achieving these goals will enable fundamental breath measurements to be made. Success in the task will require collaboration among device developers, experts in breath analysis, and clinicians.

2 Overview of Breath Analysis

The concept that breath contains molecules that originate from the human body has its origins in the writings of Hippocrates, the father of medicine. For example, distinctive breath odors have been used for centuries as indicators of what are now diagnosed as uncontrolled diabetes, liver diseases, kidney diseases, bacterial infections, or dental disease. The earliest publications of modern breath analysis appeared in the late 1960s and early 1970s, which was at the nascence for modern analytical chemistry. Researchers[1–4] reported some of these pioneering studies that were only possible as a result of enhanced separation of gaseous molecules by gas chromatography (GC), increased selectivity and sensitivity of GC detectors including mass or optical spectrometers. Breath analysis has enormous potential, because sampling breath is noninvasive, inherently safe to the subject, and poses minimum risk to the person collecting the sample. The only requirement to collect a breath sample is that the subject must be breathing "normally". ~~To~~ Breath samples can be collected easily and reproducibly in the field, in a clinic, at the bedside, in the operating room, or in an intensive care unit from infants to the elderly.

The ability to exchange oxygen for carbon dioxide is essential for many life forms. Generally, this gas exchange occurs at the gas alveolar-blood capillary cellular interface in the respiratory tract. Oxygen and carbon dioxide are passively transported from blood to breath or vice versa, and the diffusion of these gases is governed by their concentration gradients across the alveolar-capillary junction. Any additional molecule present in the blood or in the inspiratory air will also pass into the breath or blood respectively. The only requirement for transport in the gas phase is that molecules must exhibit significant vapor pressures. The molecular profile of breath will be determined by the composition of the inspiratory air and the volatile molecules that are present in the blood. The origins of the volatiles in blood are molecules and/or their metabolites that were inhaled previously (historical); molecules and/or their metabolites that entered the blood after dermal absorption; molecules and/or their metabolites that are contained in ingested foods and beverages; and molecules produced by cells (including viruses, bacteria, fungi, and yeasts) or tissues in the body including the mouth, nose, sinuses, airway, and the gastrointestinal tract. The breath matrix (99.99%) is a mixture of nitrogen, oxygen, carbon dioxide, water vapor, and the inert gases. The remainder of breath (<100 ppm) is a mixture of as many as 500 different compounds. The rates of excretion of molecules in breath are directly related to rates of ventilation and cardiac output. The physical and chemical properties of the molecules will also affect their rates of excretion. If a molecule is lipid (fat) soluble it could be stored in tissues not well perfused by blood, such as adipose tissue, and thereby be released more slowly than a similar molecule

0091-3286/2010/$25.00 © 2010 SPIE

with hydrophilic properties that is not stored. Moreover, as a general rule, the concentrations of molecules or metabolites in breath will be higher when their origins are exogenous (dermal absorption, inhalation, food and beverages).

Despite its promise and the fact that there have been a large number of publications on breath analysis, only a handful of tests are used clinically with a few others used for investigational purposes. Breath tests fall into two basic categories: tests that quantify molecules in breath after administration of a labeled chemical and tests that quantify molecules in breath without any prior administration of a labeled chemical.

2.1 *Administration of Labeled Chemicals*

The first group of tests is based on the detection of a metabolite after the administration of a known concentration of a labeled chemical (for a recent review of this field see Ref. 5). Carbon dioxide is the most popular metabolite; however, since it is one of major products of cellular metabolism, the drug or substrate must be labeled with carbon (^{13}C or ^{14}C) to separate it from endogenously produced carbon dioxide. Isotope ratio mass spectrometry (IRMS) or radiochemical methods can be used to quantify labeled carbon dioxide in the presence of unlabeled carbon dioxide.

Breath tests based on this approach require that the metabolism of the labeled chemical and the excretion of carbon dioxide be well characterized. Moreover, the breath test must be performed under defined conditions based on the time of administration of the labeled chemical and the time the breath test is administered. Additionally, the depth and frequency of breathing (ventilation pattern) of the patient must be carefully controlled. Table 1 summarizes clinical breath tests that have been proposed based on the quantification of labeled carbon dioxide.

The second group of breath tests is based on quantifying the concentration(s) of molecule(s) or groups of molecules that are produced endogenously as a result of normal physiologies.

2.2 *Endogenous Breath Molecules*

2.2.1 *Hydrocarbons*

Isoprene (2-methyl-1,3-butadiene), the most abundant hydrocarbon in human breath, was first identified[6] in adults in 1969. The biosynthesis of isoprene from DL-mevalonate was demonstrated in the cytosolic fraction of rat liver[7] and confirmed in humans[8] by showing that levels of isoprene in exhaled breath can be lowered by administration of a pharmacological agent that blocks the enzyme 3-hydroxy-3-methylglutaryl-CoA reductase (HMGCoA reductase). HMGCoA reductase catalyzes the production of mevalonic acid and is the rate-limiting intermediate in the pathway of cholesterol biosynthesis. The concentration of breath isoprene can be a noninvasive marker of endogenous cholesterol status and used diagnostically to identify human subjects who have increased risk for coronary artery disease as a result of increased biosynthesis of cholesterol such as hyperlipidemia or hypercholesterolemia.[9] Breath isoprene is a biomarker of biosynthesized cholesterol since food cholesterol does not affect the concentration of breath isoprene. Additionally, we showed that the concentration of isoprene in breath is age dependent; it is nondetectable in the breath of neonates and increases linearly with age from approximately 6 months until it plateaus in middle age.[9] The concentration of isoprene in breath decreases with old age. A similar age-dependence is known for serum cholesterol. The concentration of breath isoprene is also higher in the breath of males as compared to the concentration of isoprene in the breath of females, but this gender difference disappears after menopause.[9] Serum cholesterol reduction therapy with

Table 1 Clinical breath tests based on administration of a labeled chemical.

Labeled Chemical	Clinical Test
acetate	orocecal transit time
alanine	liver functional reserve
aminopyrene	liver function
caffeine	liver function
cholesteryloctanoate	maldigestion
diazepam	liver function
erythromycin	liver function
fructose	liver functional reserve
galactose	liver function, liver cirrhosis
glucose	insulin resistance
glycine	glycine encephalopathy
glycocholic acid	bacterial overgrowth
glycosyl ureides	orocecal transit time
α-keto-isocaproic acid	liver mitochondrial function
linoleic acid	fatty acid metabolism
methacetin	liver function, liver cirrhosis
methionine	liver mitochondrial function
mixed triacetylglycerols	fat digestion
octanoic acid	liver function, gastric emptying
ornithine	liver functional reserve
palmitic acid	pancreatic exocrine insufficiency
phenacetin	liver function
phenylalanine	phenylalanine hydrolase activity
sodium bicarbonate	hypercapnia, atrophic gastritis
D-sorbitol	bacterial overgrowth
trioctanoin	pancreatic exocrine insufficiency
triolein	fat malabsorption
tyrosine	liver function
uracil	dihydropyrimidine dehydrogenase activity
urea	*Helicobacter pylori* infection
xylose	bacterial overgrowth

pharmacological agents can be followed with breath isoprene. Levels of breath isoprene change more rapidly than serum levels of cholesterol and the patient acts as his or her own control.

Other hydrocarbons (methane, ethane, ethylene, and 1-pentane) and hydrogen have also been identified in breath. Colonic bacteria metabolizing carbohydrates that were not absorbed in the small bowel produce methane and hydrogen. Elevated levels of methane and hydrogen can therefore be used to diagnose the presence of carbohydrate malabsorption syndrome.

Ethane, ethylene, and 1-pentane have been shown to be produced by lipid peroxidation based on *in vitro* and *in vivo* studies with mouse liver and brain tissue or mice exposed to carbon tetrachloride, a known hepatotoxin and generator of free radicals.[3] Lipid peroxidation is a chain reaction with initiation, propagation, and chain termination steps. It is initiated by a reactive oxygen species, typically the hydroxyl radical, that abstracts an allylic hydrogen atom from a polyunsaturated lipid to produce a carbon-centered radical and water. This radical is conjugated, peroxidized by molecular oxygen, and undergoes a variety of reactions. Evidence of lipid peroxidation was confirmed by the reduction of the concentrations of ethane, ethylene, and 1-pentane by pretreatment of the tissue or mice with the antioxidant vitamin E. Reactive oxygen species have been implicated in the pathogenesis of many diseases from diseases of prematurity; cancer; cardiovascular, pulmonary, autoimmunological, gastroenterology, liver and kidney, neurological, and inflammatory diseases; and diabetes; to connective tissue diseases. Electron transport in mitochondria is a significant source of reactive oxygen species and cellular antioxidants are present to protect cells for oxidative damage. Approximately 2% of the oxygen used in respiration is converted to reactive oxygen species. Increased concentrations of reactive oxygen species or reduced efficiencies of antioxidant defenses have been proposed to contribute to the aging process. The field of breath ethane, ethylene, and 1-pentane is reviewed in Ref. 10.

2.2.2 *Oxygen-containing compounds*

The following oxygen-containing compounds are the major compounds that have been identified and quantified in normal human breath in order of their abundances: carbon monoxide, acetone, ethanol, acetaldehyde, methanol, and 2-propanol. Breath carbon monoxide is produced in the heme catabolism pathway and specifically is produced during the conversion of heme to biliverdin that is catalyzed by heme oxygenase 1. Carbon monoxide has been implicated in inflammatory processes, and increased concentrations of breath carbon monoxide may be evidence of the induction of antioxidant defenses.[11] Increased concentrations of carbon monoxide is also found in the breath of newborn infants with relatively immature hepatic metabolic pathways for the breakdown of hemoglobin[12] (neonatal jaundice). Breath acetone has concentrations comparable to isoprene and is the most widely studied breath molecule. Acetone is produced by liver cells (hepatocytes) from excess acetyl CoA. Acetoacetate and D-ß-hydroxybutyrate are the other species that are also produced concomitantly with acetone, and these species are known collectively as ketone bodies. Ketone bodies diffuse from hepatocytes into the blood stream and are oxidized via the Krebs cycle in peripheral tissue. Under normal conditions there is a steady state low concentration of ketone bodies in the blood and hence in the exhaled breath. In times of stress, such as during intense exercise, dieting, fasting, or starving (when fat tissue is used as an energy source instead of carbohydrates), the rate of production of ketone bodies exceeds the rate of utilization by peripheral tissues and the subject becomes ketonemic. The blood concentrations of ketone bodies are also increased with uncontrolled diabetes mellitus or chronic alcoholism. The concentrations of breath acetone have been proposed to be useful in the management of diabetes especially when used in conjunction to the determination of serum glucose.[13] The combination of these two was proposed since breath acetone was a more sensitive indicator of poor control of diabetes than of serum glucose.

Also, 2-propanol has been found in the breath of normal human subjects although at a lower concentration than acetone.[14] The origin of 2-propanol has been postulated to be the enzyme-mediated reduction of acetone; 2-propanol has been observed in ketonemic subjects who have elevated ratios of nicotinamide adenine dinucleotide and its reduced form ($NADH/NAD^+$). The potential clinical use of breath 2-propanol is limited since this molecule is present at high concentrations in most clinical environments.

Ethanol is normally found in human breath albeit at concentrations of orders of magnitude less ~~that~~ the levels of ethanol found in the breath of intoxicated subjects. The source of this ethanol is intestinal bacteria that synthesize and metabolize ethanol. Elevated concentrations of ethanol in the breath of mice have been related to obesity,[15] and the concentration of breath ethanol was reduced when the mice were treated orally to a poorly absorbed antibiotic (neomycin). This animal model suggests that obesity is a risk factor for the development of fatty liver disease or nonalcoholic steatohepatitis (NASH) in abstinent obese humans. Reduced intestinal motility in obesity may increase the potential for the gut flora to produce ethanol, may increase gut permeability, or may favor bacterial overgrowth. Increased breath ethanol may provide important information on the pathogenesis of NASH.

The origin of acetaldehyde found in normal human breath is probably the oxidation of endogenously produced ethanol since the concentration of acetaldehyde is always much lower than ethanol. Abstinent men with the low-activity polymorphism of alcohol dehydrogenase (ADH) or with low-activity polymorphism of aldehyde dehydrogenase (ALDH) were found to have high endogenous concentrations of ethanol or acetaldehyde, respectively, in their blood.[16] Concentrations of breath ethanol or acetaldehyde could be a simple way to identify humans with specific polymorphisms.

The origin of breath methanol may also be intestinal bacterial flora or methanol may be produced in any tissue when the leaving methyl groups are hydrolyzed.[17] Examples are the conversion of S-adenosylmethionine to S-adenosylhomocysteine in various tissues. No studies have reported breath profiles in human subjects with genetic defects in amino acid metabolism, although this is a potential application of a methanol breath test.

2.2.3 *Sulfur-containing compounds*

Breath sulfur-containing compounds, hydrogen sulfide, methyl mercaptan, ethyl mercaptan, dimethyl sulfide, and dimethyl disulfide, are responsible for the characteristic sweet, musty odor found ~~on~~ the breath of patients with severe

liver disease (cirrhotic patients) or patients with severe periodontal disease. The former characteristic odor known as fetor hepaticus has been characterized,[2] and the origin of these sulfur compounds was the incomplete metabolism of methionine. The degradation of methionine occurs in liver mitochondria although the transfer of an amine group from one molecule to another (transamination) pathway in the liver is not completely defined. The production of methyl mercaptan and other volatile sulfur compounds requires the presence of either glyoxylic acid or 2-oxoglutaric acid and pyruvate, and the branched chain 2-oxyacid dehydrogenase complex probably controls the transaminative flux of these compounds. Degradation of methionine can also occur in the gut by the action of bacterial methionine gamma-lyase, although the gut is not the source of methyl mercaptan and dimethyl sulfide in liver disease. Under normal circumstances, there are low concentrations of circulating sulfur-containing compounds present in the blood and breath of humans with normal, healthy livers. However, since impairment of liver function increases the level of reduced sulfur containing compounds, liver disease must affect the hepatic oxidation more than it affects transamination pathway. Metabolism of proteins by bacteria also produces elevated concentrations sulfur-containing compounds. Therefore, elevated levels of reduced sulfur compounds in breath can be used as evidence of severe periodontal disease.

2.2.4 *Nitrogen-containing compounds*

The current resurgence of interest in breath analysis follows directly from the pioneering research that identified nitric oxide as an endothelial-derived relaxant factor and showed that nitric oxide played critical roles in numerous physiological processes and in the pathophysiologies of various diseases states.[18] These studies and the direct measurement of nitric oxide in breath[19] were the catalyst for many studies that related nitric oxide in breath to pulmonary diseases. Initially there was a wide divergence of results until it was established that the nose was a significant source of nitric oxide. Understanding the role that nitric oxide plays in the mechanism of asthma has led to the establishment of international task forces that developed recommended procedures to quantify nitric oxide *in vivo*.[20–22] Another reason for the popularity of breath nitric oxide is the availability of monitors designed ~~the~~ to measure this molecule. The availability of instrumentation and the recommended measurement protocols have spurred clinical interest in breath nitric oxide, and there are thousands of publications that quantify the concentration of this gaseous radical in pulmonary diseases.

In healthy subjects, 20% of the daily production of urea is secreted into the small bowel and metabolized by bacteria to ammonia and carbon dioxide. This ammonia is subsequently reabsorbed from the intestine into the blood stream and converted by the liver back into urea. Under normal circumstances humans reuse most of the ammonia derived from catabolism of amino acids in the urea cycle although some urea, uric acid, and free ammonia is excreted in the urine. In end-stage kidney disease (uremia), urine excretion is minimal and the concentrations of the catabolites of amino acids increase in the blood. The characteristic odor of uremic breath is due to elevated levels of dimethylamine and trimethylamine.[23] Ammonia has been positively identified and quantified in the breath of normal and uremic patients using real-time mass spectrometry.[24] Uremic patients had elevated levels of ammonia compared to normal subjects. The concentration of breath ammonia can be used to examine the efficacy of renal dialysis. Elevated breath ammonia may also be exhibited in individuals with urea cycle abnormalities or liver disease (cirrhosis).

Table 2 lists some of the molecules found in human breath, their center vibrational absorption band in the mid-IR, their physiological bases, and their typical concentrations. Most of the molecules at significant concentrations in breath absorb in this spectral region with the exception of hydrogen. The breath matrix consists of approximately 5% water and 5% carbon dioxide and the vibrational absorption spectra of the breath matrix will define the region of the IR spectra available for quantification of breath molecules. Inspection of this information shows that metabolism is the major source of breath molecules and also that mouth or gut bacteria make significant contributions.

2.3 *Summary of Breath Biomarkers*

Unique breath biomarkers can only originate from the ingestion, inhalation, or absorption of exogenous substances or be metabolic products produced by foreign cells (bacteria, viruses, yeasts, or fungi). Normal cellular biochemistry can only be induced or suppressed by abnormal physiologies and although some disease states may appear to be producing unique molecules, these results are only a reflection of the detection limit of the analytical method. Differentiation between normal and disease states may be made when a particular breath molecule exceeds or is depressed below a given level or when the profiles of the concentrations of a group of molecules differ from healthy breath concentration profiles. This conclusion requires that the concentration profiles of breath molecules be established for normal healthy human subjects. Currently this information is not generally available, and it is expected that the availability of breath sensors can play a major role in solving this deficiency. Determining the normal concentration ranges of breath molecules will require that thousands of healthy subjects be studied on multiple days.

The concentration profiles of breath molecules are dynamic and change over a breath cycle. A typical breath frequency for relaxed tidal breathing is 10 or 12 breath/min. The first part of the exhaled breath comes mainly from the anatomical dead space and this volume is ~1 ml/lb of the ideal body weight. The remainder of the breath is called mixed expired. The volume of gas exhaled over a single breath is known as the tidal volume, and minute ventilation is the volume of gas exhaled during 1 min. Minute ventilation must provide enough oxygen to the lung epithelial cells to meet the metabolic demands of all the body tissues. Hyperventilation or hypoventilation provides more or less than the required amount of oxygen to the lung. The concentration profiles of breath molecules in dead space air corresponds to the atmospheric composition, i.e., ~21% oxygen and 0.4% carbon dioxide, whereas the main concentration profiles of mixed expired air consists of ~17% oxygen, 5% carbon dioxide, and 5% water vapor.

2.3.1 *Breath sampling*

If breath analysis is to be used in ~~the field of~~ clinical analysis it must either provide novel information not provided by existing techniques or else provide results in a shorter

Table 2 Typical molecules found in normal human breath.

Compound	Vibrational Absorption (μm)	Concentration Range (v/v)	Physiological Basis
acetaldehyde	9.8–9.2	ppb	ethanol metabolism
acetone	7.3	ppm	decarboxylation of acetoacetate
ammonia	10.3	ppb	protein metabolism/bacterial metabolism
carbon dioxide	4.2	%	respiration
carbon monoxide	4.7	ppm	heme catabolism catalyzed by heme oxygenases
carbonyl sulfide	4.9	ppb	gut bacterial oxidation of reduced sulfur species
ethane	3.3, 6.8	ppb	lipid peroxidation
ethanol	9.8–9.2	ppb	gut bacterial metabolism of sugars
ethylene	10.6	ppb	lipid peroxidation
hydrogen	Not feasible in IR	ppm	carbohydrate metabolism
hydrogen sulfide	1.6, 2.7, 3.7, 7.7–7.9	ppb	anerobic bacterial metabolism of thiol proteins
isoprene	11.1	ppb	cholesterol biosynthesis
methane	3.3; 7.9	ppm	gut bacterial metabolism of carbohydrates
methanethiol	3.45–3.28	ppb	methionine metabolism
methylamine	12.2	ppb	protein metabolism
nitric oxide	5.3	ppb	involved in vasodilatation, or neurotransmission; production catalyzed by nitric oxide synthases
1-pentane	6.8	ppb	lipid peroxidation
water	everywhere	%	respiration

period of time. Real-time breath analysis will compete successfully with conventional blood or tissue assays since the diagnoses could be made earlier and treatment initiated. Quantum cascade lasers (QCLs) and interband cascade lasers (ICLs) provide the potential for real-time analysis and for the development of portable devices. It is reasonable to propose that the sampling method for all monitors that use QCLs or ICLs will involve monitoring a single breath similar to the standard maneuver that is used for online breath nitric oxide analysis.[20–22] An example of the breath sampling using this standard maneuver[25] is shown in Fig. 1 The nitric oxide signal in Fig. 1 (solid line) begins to rise as the breath is exhaled. The mouth pressure (dotted line) is achieved almost instantaneously, but there is a slight delay in the response of the nitric oxide chemiluminescence detector (NO Analyzer 280, Sievers Instruments). After a few seconds of exhalation at a mouth pressure of 10 cm H_2O and a constant flow of 50 ml/s, a signal is recorded. Constant flow is achieved by use of a critical orifice, and the subject, with visual coaching, maintains a constant mouth pressure. Simultaneously, carbon dioxide should be monitored with a commercial capnograph. The profiles of carbon dioxide and the mouth pressure as a function of exhalation define the quality of the breath sample and establish whether there are different tissue or cell sources of the breath biomarker.

2.3.2 *Background contaminants*

The composition of the inspiratory air contributes significantly to breath analysis. Many potentially clinically relevant molecules are present in the ambient environment. Currently,

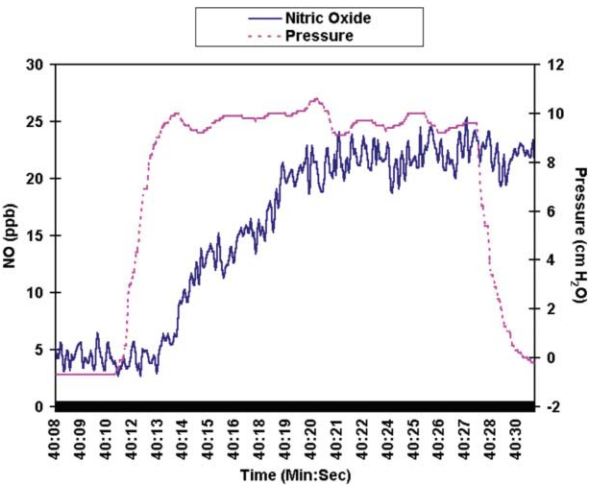

Fig. 1 Nitric oxide and mouth pressure signals from a single breath exhalation.

there is no consensus for a standard method to enable the background levels to be subtracted. At least part of the reason for this deficiency is the fact that there are no data that define how long it takes for a subject to reach steady state with his or her ambient environment. It has been suggested the lung can be washed out in approximately 4 min if a subject breathes pure air.[10] However, the washout of the entire body may take days or weeks, depending on the identity of the molecule. Consequently, the body may take a significant time to reach steady state with the composition of inspiratory air. Analytical data should be treated with caution when a sample of inspiratory air is greater than 25% of the concentrations in breath. This limitation is proposed since the study subject may not be in steady state with his or her environment, and the resulting analysis will have a significant error.

2.3.3 *Reporting concentrations of breath biomarkers*

Interlaboratory guidelines should also define the way the results of breath analysis are expressed so that intrasubject and intersubject breath analyses can be compared and contrasted. Breath analysis for single breath samples could be expressed in terms of concentration units that are dimensionless (i.e., parts per million etc.) or in terms of moles per unit volume (picomoles per liter). Alternatively, single breath analyses could be normalized to a physiological based parameter such as carbon dioxide production (i.e., picomoles per ~~liter~~ L of CO_2) or oxygen consumption (i.e., picomoles per milliliter of O_2). Normalization to carbon dioxide or oxygen enables breath analysis data for subjects with widely different body masses to be compared.[26,27]

3 Overview of Mid-IR QCL- and ICL-Based Breath Analyzers

QCLs and ICLs are convenient mid-IR sources for ultrasensitive and highly selective trace gas monitoring as the result of recent advances in the technologies of their fabrication. They can be fabricated to operate over a wide range of wavelengths from ~3 to ~20 μm. Absorption spectra in the mid-IR of several small molecules of potential interest for trace gas monitoring are depicted in Fig. 2. The upper panel shows absorption spectra in the atmospheric window between the bending fundamental of water centered at around ~1600 cm^{-1} and the water OH stretches starting above 3200 cm^{-1}. The lower panel shows absorption spectra in the atmospheric window below the water bending fundamental. The logarithmic ordinate scales are the integrated intensities of the lines on a per molecule basis. Continuous wave (cw) QCL devices capable of thermoelectrically cooled, room-temperature operation with a number of important practical features, including the single-mode emission with mode-hop-free frequency tuning, high power (tens to hundreds of milliwatts), and intrinsic narrow emission line width are available in the 4- to 12-μm spectral region.[28] These spectral characteristics enable the development of compact, robust trace gas sensors.[29–32] For example, the Rice Laser Science group has explored the use of several methods for carrying out infrared laser absorption spectroscopy (LAS) with mid-IR QCL and ICL sources, which include multipass absorption spectroscopy,[29] cavity ring down spectroscopy[33] (CRDS), integrated cavity output spectroscopy[34] (ICOS), as well as photoacoustic spectroscopy (PAS) and quartz-enhanced photoacoustic spectroscopy[28,35] (QEPAS). LAS is an extremely effective tool for the detection and quantification of molecular trace gases with demonstrated detection sensitivities ranging from parts per million by volume to parts per trillion by volume levels depending on the specific gas species and the detection method employed. These high sensitivities are obtained using fundamental vibrational molecular absorption bands accessible in the mid-IR spectral region. Section 3.1 describes the properties of QCLs and ICLs including widely tunable QCL/ICL sources, which are expected to impact the research and development of commercial breath analyzers. This is be followed by a discussion of the specific requirements of exhaled trace gas sensors and the various methods for improving sensitivity including the Rice PAS/ QEPAS technology. Several specific applications of QCLs/ICLs to breath analysis are described in Sec. 4.

3.1 *Properties of Quantum and Interband Cascade Lasers*

High optical power and single-frequency operation with good spectral purity and wide wavelength tunability of the laser source are the most critical characteristics for exhaled gas sensing using spectroscopic techniques. A QCL with its cavity formed by Fresnel reflections at its end facets typically operates simultaneously in multiple longitudinal modes. Single-frequency operation is usually achieved by introducing a distributed feedback (DFB) structure into the QCL active region to favor a particular mode. Typically, the maximum tuning range of DFB-QCLs achieved by changing the laser injection current is 3 to 4 cm^{-1}. This can be increased to ~20 cm^{-1} by varying the temperature of the QCL chip. Because of the limited tuning range and the precision required in the fabrication of the embedded DFB structure, obtaining a DFB-QCL that operates at precisely the desired wavelength is presently still technically challenging. However, once obtained at the right wavelength, a mid-IR DFB-QCL has the significant advantage of being very compact and robust, making it very useful for monitoring a specific trace gas with resolved rotational structure from small molecular species. However, a DFB-QCL, with its limited spectral tuning range, is not useful for monitoring a gas with a congested rotational spectrum by laser spectroscopy, since it is difficult to scan sufficiently far to ascertain the band profile of a congested absorption band.

However, the spectral width of the QCL optical gain profile is usually significantly broader than 20 cm^{-1}, and therefore QCLs can provide in fact a much broader wavelength tuning range. Recent advances have resulted in very broad gain profiles. The bound-to-continuum QCL design first proposed by Faist et al.[36] and the heterogeneous QC structure first demonstrated by Gmachl et al.[37] as a supercontinuum QCL, are the most promising structures in terms of broadband emission, and have been further developed for wide single-mode-frequency tuning spectroscopic applications.[38–42]

To take advantage of the broadband gain of such QCLs, an external cavity (EC) configuration can be used to obtain single-mode operation at any wavelength within the laser gain profile. A widely tunable QCL spectrometer implementing a novel EC-QCL architecture for high-resolution spectroscopic applications and multispecies trace-gas detection was demonstrated[41] with a thermoelectrically cooled Fabry-Pérot gain medium operating in a cw mode at λ ~5.28 μm such an instrument depicted employs a piezoactivated cavity mode tracking system for mode-hop-free operation.

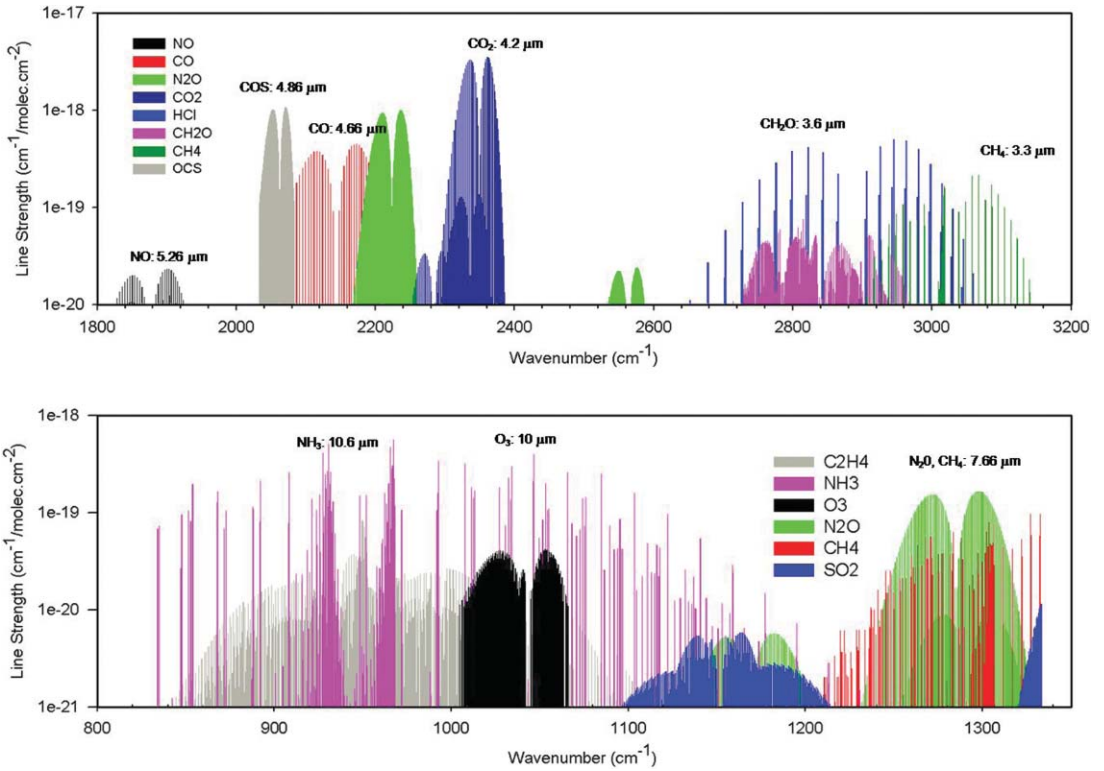

Fig. 2 HITRAN simulation of absorption spectra of simple molecules.

The mode-tracking system provides independent control of the EC length, diffraction grating angle, and laser current. The QCL gain medium enabled a coarse laser frequency tuning range of ~155 cm^{-1} and a high-resolution (better than 0.001 cm^{-1}) continuous mode-hop-free fine-tuning within a range of up to 2 cm^{-1} with a maximum available optical power of ~11 mW.

Wide wavelength tunability around $\lambda = 5.28\ \mu m$ enables accessing most of the absorption lines within the fundamental vibrational band of NO. A laser linewidth of <30 MHz, which enabled resolving spectral features separated by ~0.01 cm^{-1} makes a tunable mode-hop-free EC-QCL an excellent light source suitable for high-resolution spectroscopic applications and multiple species trace-gas detection. The flexibility of this arrangement makes it possible to use it with any QCL gain media without requiring an embedded DFB structure and at any mid-IR wavelength without changing the EC configuration, except for some wavelength-sensitive components.

More recently, the use of a metal oxide chemical vapor deposition (MOCVD)-grown buried-heterostrusture Fabry-Pérot QCL gain medium operating at $\lambda = 8.6\ \mu m$ in the already described EC-QCL sensor architecture resulted in considerably higher levels of optical output power. The maximum single-frequency output power obtained in the EC-QCL configuration was 190 mW. Commercial pulsed and cw, room-temperature mid-IR EC-QCLs are available from Adtech Alpes Lasers, Daylight Solutions, Inc., and Hamamatsu with output powers ranging from 30 to 350 mW and frequency tuning ranges from 60 to 430 cm^{-1} from 4.3 to 10.5 μm (Ref. 27).

Until now we have considered only intersubband QCLs. The other type of mid-IR lasers are ICLs. These are a hybrid of a diode laser and a cascade laser. The lasing transition occurs when a conduction band electron confined in a quantum well of one material annihilates a quantum confined hole in the valence band of a different material emitting a photon. This is similar to a diode laser in that it involves an interband transition, although with diode lasers only a single material is typically involved. In a diode laser, each electron is used only once, whereas in an ICL, an electron in the valence band well tunnels out and is raised in energy through a series of quantum wells until it possesses sufficient energy for the lasing transition process to be repeated. Thus, the same electrical current is used repeatedly in a cascade process. Because ICLs have bandgap energy available, they operate at shorter wavelengths than QCLs, typically in the 3- to 4-μm spectral region.[43–45] ICLs are more difficult to fabricate, but they enable access to shorter mid-IR wavelengths, which are particurly effective for the ~~dedection~~ detection of such biomarkers as methane and ethane.

3.2 *Fundamentals of Exhaled Trace Gas Sensing*

Generally, detection sensitivity, selectivity, and response time are the primary requirements for trace gas sensing. For small molecules with resolved rotational structure, selectivity is obtained by choosing an absorption line that is free of interference from other species that might be present in the sample. Furthermore, reducing the sample pressure sharpens the absorption line without reducing the peak absorption until the linewidth begins to approach the Doppler width. This sharpening of the absorption line also significantly improves selectivity. To obtain the best sensitivity, a strong molecular absorption line must be selected, and a long effective optical path length must be used. High sensitivity requires that absorption from baseline variations and laser

power fluctuations can be identified. The first requirement is best met by choosing a line in a fundamental absorption band as such a line tends to be stronger than a line in near-IR overtone or combinations bands. An effective long optical path length can be obtained by using multipass cells or cavity enhancement techniques. For sharp absorption lines, noise associated with laser power fluctuations can be greatly reduced by averaging rapid scans over the line or by a similar wavelength modulation technique. The final requirement to distinguish absorption from baseline variations is the most challenging. Every multipass sensor configuration exhibits accidental étalons, which typically have widths comparable to the absorption line width. In principle, these can be removed by evacuating the cell, replacing a sample gas by a gas without absorption (i.e., "zero air" or ultrapure nitrogen) and then dividing the sample trace by this background trace. This approach assumes that accidental étalons do not shift their pattern during the process of sample replacement.

Large molecules do not have resolved rotational structure, as mentioned previously. Molecules with four heavy atoms or low-frequency vibrational modes typically are enough to cause congested spectra. Because there is no nearby baseline to compare with, one way to detect absorption is also by pumping the sample out and replacing it with zero air. For weak absorptions expected for trace gas concentrations this imposes severe limits on long-term power stability of the laser source, the absence of low-frequency laser noise, and baseline stability. Without a sharp rotational spectral component, the required long-term power stability is typically ~ 1 in 10^4. Furthermore in the mid-IR fingerprint region, where many gases absorb, there may be other gases contributing to a broad absorption, putting selectivity in jeopardy. As we shall see in Sec. 3.2.3, the advantage of PAS is that power and baseline stability requirements are reduced.

3.2.1 *LAS based on multipass gas cells*

Combining mid-IR QCLs with the techniques of long-path-length absorption spectroscopy provides a flexible and straightforward route to high sensitivity and high-precision measurements of a wide variety of gas phase molecules. Increasing the absorption path length is a universal method of increasing the absorption depth, and thus, the sensitivity of spectroscopic measurements. The long path length generally is provided by a multipass cell, an optical device that folds the path into a compact volume. Common types of multipass cell include the White cell,[46] the Herriott cell,[47] and the astigmatic Herriott cell.[48] The basic configuration of a long-path-length spectrometer is quite simple, comprising a laser, followed by a multipass cell, and then a detector. The basic measurement of the absorption involves a comparison of three quantities, the signal at zero light, the signal due to background light (on either side of the absorption), and the light signal centered on the absorption line. The limiting noise source may be detector noise (with low optical power) or noise associated with the light, such as laser noise or fluctuations of optical interference fringes produced in the multipass cell.

3.2.2 *Cavity enhanced techniques*

Another way to obtain a very long path length is through application of resonant optical cavities instead of using multipass cells, CRDS, sometimes also referred to as cavity leak out spectroscopy[33,49–55] (CLEOS), is intrinsically background free. When carried out with high-power pulsed lasers, it is very simple to implement, requiring in addition to the laser, only high-quality cavity mirrors, a reasonably fast detector, and suitable data acquisition. However, this technique is harder to implement with QCLs, which have maximum pulse powers only a few times their cw output. At the cost of additional complexity, this power limitation can be overcome by locking the cavity to the laser to fill the cavity followed by rapid laser turn off. Alternatively, the cavity can be dithered while a cw laser is scanned slowly. All of these approaches are hindered by short ring-down times.

A more common method has been the direct measurement of light absorption by the sample in the cavity. To avoid the requirement that the cavity and laser must be locked together, an effective approach has been to use off-axis integrated cavity output spectroscopy[34,56–58] (OA-ICOS). This method is very closely related to LAS using a multipass cell with the principal difference being that in ICOS, the beams are allowed to overlap on the mirrors after many passes through the cavity, thereby exciting high-order cavity modes. Another approach for removing mode noise in OA-ICOS is to vibrate the mirrors. This causes many mode hops to occur within the time required to empty the cavity, effectively averaging out this noise. Since there are no transparent holes in the mirrors used in ICOS to admit and allow the exit of the laser beam, ICOS requires more laser power, which is obtainable with QCLs. A medical application of QCL-based OA-ICOS is the measurement of NO and CO_2 in breath.[59]

3.2.3 *PAS and QEPAS*

PAS is based on the photoacoustic effect, in which acoustic waves are produced by the absorption of modulated laser radiation by target trace gas species. By the use of an acoustic cell, which is acoustically resonant at the modulation frequency, this is an effective method for sensitive trace gas detection. In contrast to other IR absorption techniques, PAS is an indirect technique in which the effect on the absorbing medium and not the direct light attenuation is detected. Light absorption results in a transient temperature effect, which translates into pressure variations in the absorbing medium that can be detected with a sensitive microphone. PAS is ideally a background-free technique, since only the absorbing gas generates the signal. However, background signals can originate from nonselective absorption of the gas cell windows (coherent noise) and external acoustic (incoherent) noise. PAS signals are directly proportional to the pump laser power and therefore maximum detection sensitivity can be realized conveniently with the thermoelectrically cooled (TEC) high-power QCLs and ICLs described in Sec. 3.1.

A novel approach to photoacoustic detection of trace gases utilizing a quartz tuning fork (QTF) as a sharply resonant acoustic transducer was first reported[27,59,60] in 2002. The basic idea of QEPAS is to invert the common PAS approach and accumulate the acoustic energy not in a gas-filled acoustic cell but in a sharply resonant acoustic transducer. A natural candidate for such a transducer is crystal quartz, because it is a low-loss piezoelectric material. A nearly optimum commercially available quartz transducer can be found in a QTF (see Fig. 3). QTFs typically resonate at 32,768 (2^{15}) Hz in electronic clocks as frequency standards. A schematic of the QEPAS absorption detection module or "spectrophone"

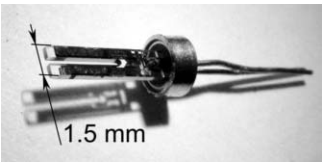

Fig. 3 Photograph of a QTF QTFs of this geometry was used in most QEPAS studies carried out at Rice University.

consisting of a QTF equipped with an acoustic microresonator is depicted in Fig. 4. In its simplest configuration [Fig. 4(a)] the laser radiation is focused between the prongs of the QTF and its wavelength is modulated at a $f_m = f_0/2$ frequency or its intensity is modulated at the $f_m = f_0$ frequency (where f_0 is the QTF resonant frequency), depending, respectively, on whether wavelength modulation or amplitude modulation of the laser is used. The acoustic wave at f_0 induced by absorption of the laser by the gas becomes the driving force to excite the antisymmetric fundamental mechanical vibration of the QTF prongs (i.e., the two QTF prongs move in opposite directions). Sound waves from distant acoustic sources tend to move the QTF prongs in the same direction, which results in zero net piezocurrent, thus, making this element insensitive to such excitation. The electrical signal produced by this piezoelectrically active mode of vibration is picked up by two pairs of electrodes deposited on the QTF prongs and measured using lock-in detection at f_0. Spectral data can be acquired by scanning the laser wavelength. To increase the effective interaction length between the radiation-induced sound and the QTF, a gas-filled acoustic microresonator [see Fig. 4(b)] can be added similarly to the traditional PAS approach. It was shown experimentally that the configuration [Fig. 4(b)] yields up to 30 times improvement of the signal-to-noise ratio (SNR) compared to configuration in Fig. 4(a), depending on the gas composition and pressure. Other QEPAS spectrophone configurations are also possible, such as off-beam QEPAS (Ref. 19).

Advantages of QEPAS compared to conventional PAS include small size comparable with a semiconductor laser; sensor immunity to environmental acoustic noise (sensitivity is limited by the fundamental thermal QTF noise); a simple and low-cost absorption detection module (spectrophone); a high Q factor (typically ~10,000 at atmospheric pressure); a large dynamic range (10^9) from thermal noise to breakdown deformation; wide temperature range up to 700 K, where the piezoelectric effect of quartz vanishes; and the capability to analyze small gas samples down to a few cubic millimeters in volume. The pressure corresponding to optimum sensitivity depends on the V-T energy conversion cross section of the gas of interest. It was experimentally found that this optimum pressure for fast-relaxing molecules with resolved optical transitions is ~50 Torr, which also ensures Doppler-limited spectral resolution. For slow to relaxed gases such as NO or CO, this optimum pressure is higher.

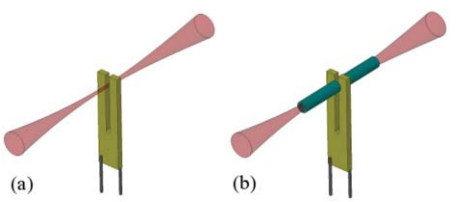

Fig. 4 QTF-based spectrophones: (a) simplest configuration and (b) improved configuration with an acoustic resonator formed by two pieces of rigid tubing.

QEPAS sensor technology has already been demonstrated in trace gas measurements of 15 target analytes, including NH_3 (Ref. 61), CO_2 (Refs. 62 and 63), N_2O (Ref. 64), COS (Refs. 65 and 66), and HCN (Ref. 67), and HCHO (Refs. 68 and 69). The lowest normalized noise equivalent absorption coefficient of 1.9×10^{-9} cm^{-1} W Hz$^{-1/2}$ was obtained[70] for H_2O using QEPAS. This figure of merit is comparable to the best conventional PAS results. An experimental study of the long-term stability of a QEPAS-based NH_3 sensor showed that the sensor exhibits very low drift, which enables long-term data averaging (>3 hs). This can provide a significant improvement of the SNR in concentration measurements as the SNR scales as $\sqrt{t}$.

QEPAS excitation can also be performed in an amplitude modulation (AM) mode, and in this case, a coherent acoustic background is present. This background is directly proportional to the laser power reaching the spectrophone. Therefore, the sensitivity limit is no longer determined by the QTF thermal noise alone but by the laser power fluctuations and spurious interference features. The AM mode must be used if the absorption feature of interest is spectrally so wide that fast modulation of the laser wavelength across this feature is not possible. This is the case for the large or heavy molecules listed in Table 1, when the individual rotational-vibrational transitions are not resolved and absorption bands look unstructured. The performance of an AM 8.4-μm QCL-based QEPAS sensor system that demonstrated the detection of broadband absorbing target species in the mid-IR spectroscopic fingerprint region was reported in Ref. 71. Using a similar approach, we developed[72] a QEPAS sensor employing an EC-QCL targeting the unresolved absorption spectrum of C_2HF_5 (freon 125) at λ~1150 cm^{-1}. The laser source exhibits single-frequency tuning of 180 cm^{-1}. In this sensor, a photoacoustic signal is generated by turning the laser on and off at the exact resonance frequency of the applied QTF. The sensitivity of this AM-QEPAS-based sensor was determined both for single-point measurement as well as in a broadband wavelength scan using a calibration mixture of 15 ppm freon-125A in dry nitrogen. With a laser frequency set to 1208.62 cm^{-1}, which corresponds to the maximum absorption of freon 125 in this spectral region, continuous concentration measurements were performed. A minimum detection limit (1σ) of ~9 ppb was calculated for these conditions based on the scatter of the background signal measurements. The power and measurement bandwidth normalized noise equivalent absorption coefficient (NNEA) of this sensor was determined to be 7.92×10^{-9} cm^{-1} W Hz$^{-1/2}$ for freon 125. The applied cw TEC EC QCL provided ~50 mW of optical power. This corresponds to a minimum detection absorption coefficient limit for C_2HF_5 of $\sim3.2\times10^{-7}$ cm^{-1} with 1-s averaging time.[72]

4 Exhaled Trace Gas Sensing Examples

4.1 *NO Using a High-Finesse Optical Cavity*

Several techniques exist to perform high-sensitivity absorption spectroscopy in a high-finesse optical cavity, as already mentioned previously in Sec. 3, such as laser absorption spectroscopy,[73–75] CRDS or ICOS. In these techniques, the

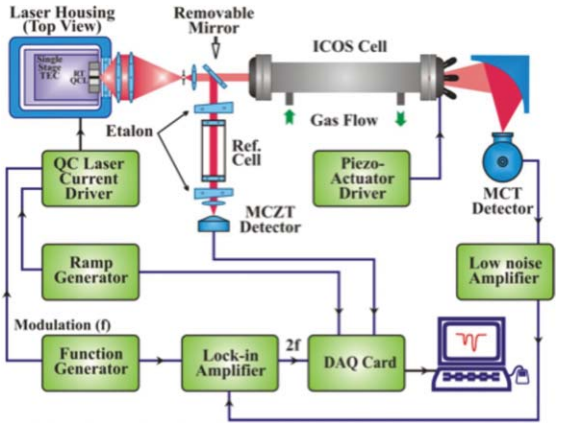

Fig. 5 A cw-TEC-DFB QCL based OA-ICOS sensor platform.

coupling efficiency of the laser radiation into the resonant cavity is extremely critical and determines the amount of light that can be collected by a photodetector placed after the absorption cell. In an off-axis ICOS (OA-ICOS) arrangement, in which the optical system is aligned in such a way that the maximum number of longitudinal and transverse modes is excited within the cavity, the typical optical throughput[55] of the cavity is of the order of $\leq T/2$ (where T is transmission of the cavity mirrors). In this case, the system requires a very sensitive detector so as not to be limited by the detector noise floor. Therefore, these techniques can also benefit from the increased laser power available from cw, high-power QCLs, which results in substantial improvement of their detection sensitivity and/or enable us to use less sensitive, but TEC detectors, which is critical in a field-deployable gas sensor system.

A nitric oxide sensor based on a TEC, cw DFB QCL laser operating at $\lambda = 5.45\ \mu$m (1835 cm^{-1}) and OA-ICOS combined with a wavelength-modulation technique was developed to determine NO concentrations at ~1 ppbv levels essential for detecting NO in exhaled human breath.[73,76] The sensor shown in Fig. 5 employs a 50-cm-long high-finesse optical cavity that provides an effective path length of 700 m. A noise equivalent minimum detection limit of 0.7 ppbv with a 1-s observation time was achieved. A wavelength modulated signal for a calibrated NO concentration of 23.7 ppbv was fitted using a general linear fit procedure, as shown in Fig. 6. A detection sensitivity of 0.03 ppbv was achieved with a 30-s averaging time using a multipass gas cell with an optical path length of 210 m, corresponding[76] to an absorption coefficient of 1.5×10^{-10} cm^{-1}. More recently, Aerodyne Research reported[29] a transportable fast response, QCL-LAS system capable of measuring NO as well as CO_2, CO, and N_2O. This instrument can obtain 1-s detection precisions of 0.5 to 0.8 ppbV based on LAS using state-of-the-art room-temperature, pulsed DFB QCLs with improved laser stability.

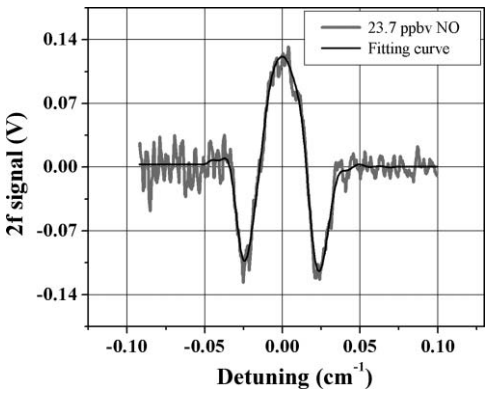

Fig. 6 Graph of 2*f* OA-ICOS-based NO absorption signal.

4.2 *NO Faraday Rotation Spectroscopy*

Faraday rotation spectroscopy[27,77–82] (FRS) takes advantage of dispersion effects of paramagnetic species (such as NO, NO_2, OH^-, or O_2). When an external magnetic field is applied in the same direction as the light propagation, paramagnetic molecules exhibit magnetic circular birefringence (MCB). This implies that the refractive index is different for left-handed and right-handed circularly polarized waves traveling in the absorbing medium. Thus, with the transition split by the magnetic field, linearly polarized light, which is a superposition of two circularly polarized waves, is affected by different Zeeman components of the transitions, and MCB can be observed as rotation of the polarization plane of a linearly polarized laser radiation. Such a polarization rotation, which is observed strongly only around absorption lines, is proportional to the column density of the paramagnetic species. The polarization rotation angle can be detected using a modulated magnetic field and phase sensitive detection techniques.

Figure 7 shows the basic FRS setup. The FRS signal is measured by placing the sample between two polarizers, so that the Faraday rotation can be detected as intensity modulation of the light emerging from the second polarizer (analyzer). Two methods have been used for polarization rotation measurement: the so called 90-deg method uses two polarizers with almost crossed polarization axes and a single photodetector for sensing of the transmitted light intensity and the second measurement method orients the analyzer at 45 deg, splitting the beam into two polarizations and uses two balanced detectors to detect ~~that~~ the beams go out of balance when MCB is present. SNR enhancement is achieved in slightly different ways for the two methods, but fundamentally both are based on efficient suppression of laser amplitude noise while maximizing the Faraday rotation signal. In both methods, the spectral shape of the FRS signal is the sum of the differences between Zeeman shifted dispersion curves. Since the polarization rotation and thus the variation of the analyzer transmission exist only when ~~the~~ NO molecules are present, FRS is considered a zero optical background technique and provides ultrahigh sensitivities.

In the 90-deg method, suppression of the laser noise is achieved by nearly crossing the analyzer, thus reducing the

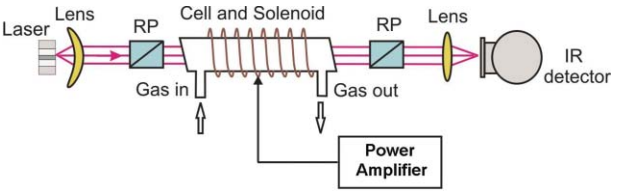

Fig. 7 Schematic of the 90-deg FRS scheme. Two Rochon polarizers (RP) are nearly crossed at an angle determined to yield the best SNR.

amount of laser amplitude noise arriving at the detector. The signal is also suppressed by crossing the polarizers, but SNR enhancement is obtained because the signal is an approximately linear function of the displacement of the analyzer angle from minimum transmitted light, while the noise has a quadratic dependence on angle. The application of QCLs exhibit much lower amplitude noise than, e.g., color center laser sources. This is an important step in adopting the FRS technology for applications outside the research laboratory.[77]

Depending on the ratio of laser intensity fluctuations to detector noise at the modulation frequency, the SNR can be limited either by detector noise for quiet sources or by polarizer quality for noisier sources. There is an optimum analyzer angle for the 90-deg method, which depends on detector noise or polarizer quality. This has been analyzed in detail (see supplementary information in Ref. 77).

The FRS signal can be modeled based on parameters of the molecular transition, including magnetic moment and experimental conditions (sample pressure, temperature, magnetic field amplitude, optical path-length, etc.). Precise modeling of the FRS signals has a great potential for providing consumable-free calibration, which is particularly attractive for field sensing applications.

An experiment using a cryogenically cooled indium-antimonide (InSb) detector with an only 44 cm optical path length yielded a 1σ minimum NO detection limit of 380 pptv with a 1 s lock-in time constant. This corresponds to 5.9×10^{-8} equivalent minimum detectible fractional absorption calculated for this NO $Q_{3/2}(3/2)$ line. The best current state-of-the-art LAS systems require more than 10 times the path length to provide a comparable sensitivity.

FRS can be applied to most molecular species possessing a permanent magnetic dipole moment. Examples are NO; oxygen; nitrogen dioxide; and many radicals, e.g., the hydroxyl radical. Semiconductor laser sources and, in particular, QCLs, which operate in the mid-IR molecular fingerprint region, in combination with ultrasensitive FRS, can provide particularly attractive technology for compact and accurate trace-gas detectors for field applications.

4.3 *Ammonia*

A QCL-based breath sensor employing a quartz-enhanced PAS technique with a detection sensitivity for exhaled ammonia at a <10 ppbv concentration level with a 0.5-s time resolution is described in Ref. 41. Typical concentrations of ammonia in healthy human breath are in the range of a few hundreds parts per billion by volume. Therefore, laser spectroscopy in combination with a mid-IR, cw, high-performance QCL is a promising analytical approach for real-time breath analysis.

More recently, we used a cw DFB QCL or a tunable EC-QCL-based QEPAS sensor and a wavelength-modulation technique. The DFB QCL operated at 5°C and provided a maximum power of ~30 mW. A tuning range of ~4.5 cm^{-1} by varying the injection current enabled the monitoring of an ammonia line at 1046.4 cm^{-1}. The EC-QCL was tuned to the 930.8-cm^{-1} NH_3 line, which is free from potential spectrally interfering species such as CO_2, H_2O, and CH_3OH. Breath ammonia measurements were performed on a healthy volunteer over a 3-week period with the DFB QCL. Performance characteristics for both the DFB-QCL and the EC-QCL sensor platforms operating with $2f$ and $1f$ wavelength modulation, respectively, were obtained.

4.4 *Carbonyl Sulfide*

A sensor was designed for simultaneous concentration measurements of COS at the parts per billion level and CO_2 at the percent level. A description of the sensor design and performance is reported in detail.[66] Elevated COS concentrations in exhaled breath have been reported in lung transplant recipients suffering from acute rejection as well as in patients with liver disease.[83,84] The TEC QCL used in this work[66] operates in a pulsed mode at 4.85 μm and can access a number of strong absorption lines (line intensities of about 1×10^{-18} cm^{-1}/molecule cm^{-2}) in the P branch of the COS fundamental rotational-vibrational spectrum. The availability of a neighboring CO_2 line within the tuning range of the QCL enables ventilation monitoring simultaneously with a COS measurement and can be used to normalize the resulting COS concentrations, and to standardize measurement conditions. To address space and safety constraints relating to a medical setting, a digital signal processing (DSP) platform for pulsed QCL-based biogenic trace gas sensors was developed to provide fast data acquisition (faster than 1 MHz), standalone data processing functions, increased reliability, and enhanced sensor portability.

4.5 *Stable Isotopes of Carbon Dioxide*

Breath tests based on the administration of ^{13}C-labeled molecules require the accurate quantification of the enrichment of the stable isotopes in breath carbon dioxide. Until now, IRMS or nondispersive infrared spectrometry (NDIRS) have been the methods of choice for quantifying enrichment. IRMS is extremely sensitive but costly and requires expert personnel to maintain and operate the mass spectrometers, whereas NDIRS is significantly less expensive and can be operated by medical personnel. Briefly, in this test the patient provides a baseline breath sample and then ingests ^{13}C-labeled molecules. A second breath sample is taken at a specific time after the ingestion of the labeled molecules. Ingestion of the enriched stable isotope causes the $^{13}CO_2/^{12}CO_2$ to increase by ~5 parts per thousand (or per milliliter) compared to the baseline value. More recently, mid-IR LAS or CRDS have been demonstrated to offer a more compact and convenient alternative method in the treatment of *Helicobacter pylori* infection first discovered in 1982 by Marshall and Warren.[54]

4.6 *Broadband Absorbers*

4.6.1 *Ethane ICL-based OA-ICOS spectroscopy*

Ethane, a breath biomarker of lipid peroxidation, has the potential for broad clinical applications. The development of a compact system using OA-ICOS with a LN_2 cooled, cw, 4-mW DFB ICL operating at 3.35 μm (2986.7 cm^{-1}) was used in real-time measurements of breath ethane.[85] The ICOS cell length was 57 cm and the mirror diameters were 5 cm with an effective internal cell volume of 630 cm^3. The ICOS cell mirrors had a specified reflectivity 99.98% and the radius of curvature was 1 m. The ethane was pumped through the OA-ICOS cell using a small oil-free diaphragm pump. A Nafion® filter was used to remove any moisture and other polar molecules that are possible interfering species. A 580-μm-diam flow-limiting orifice enables

measurements to be taken at a constant flow rate of ~ 50 standard cm^3/s. Light leaving the OA-ICOS cell was focused onto a liquid-nitrogen-cooled InSb detector using an off-axis parabolic reflector ($f = 5$ cm). The detector responsivity is 2 A/W, and was followed by amplifiers and filters with transimpedance gain of 2×10^7 V/A and a 3-dB frequency of 10 kHz, respectively. The measured dark current noise was 3 pA / $Hz^{1/2}$, and typical dc voltage was 100 mV. This implies that the detector-limited noise equivalent absorbance was $6\times10^{-4}/Hz^{1/2}$.

An ICOS cell volume (630 cm^3) and target pressure (0.17 atm = 130 Torr) resulted in an effective air volume of 108 standard cm^3. A typical healthy individual can produce ~700 cm^3 in a single exhalation, so that the ICOS cell volume is flushed ~ seven times in a single online measurement. Data acquisition electronics in a personal computer were used to tune the laser frequency with a current ramp and capture the detector output voltage. Software and a graphical user interface were developed to calculate and report running averages of absorption spectra and integrated absorbance in real time.

The ethane absorption feature of interest at ~2986.7 cm^{-1} is a group of unresolved transitions, for which the HITRAN database contains only calculated oscillator strengths and no measured data. Single-pass measurement of a calibrated mix of ethane in nitrogen (949 ppb) showed considerably weaker peak absorption than that predicted by HITRAN. The highly reflective mirrors were replaced with transparent windows for this measurement, which was made using a high concentration so that a single 57-cm path length would result in a strong absorption signal. The measured peak absorption coefficient is 1.7×10^{-3}/ppm-m at 85 Torr (> 0.1 atm).

To estimate the actual path length in the OA-ICOS cell, a calibrated low-concentration mix of 100 ppb ethane in nitrogen was measured. An effective path length $L_{eff} \approx 1350$ m was deduced, from which the inferred mirror reflectivity is $R_{eff} = 0.9996$. Combining this path length and the measured absorption coefficient (1.7×10^{-3}/ppm-m) with the detector-limited noise equivalent absorbance ($6\times10^{-4}/Hz^{1/2}$) predicts a noise equivalent detection limit of 0.13 ppb/$Hz^{1/2}$. The path length calibration was performed periodically and recorded for use in scaling the measured concentrations in the breath samples. The minimum detectable absorbance is determined by the fluctuations in the wings of the absorbance spectrum. In this case, the measured minimum detectable absorbance is $\approx7\times10^{-3}$, so that the noise-equivalent absorbance is $1.1\times10^{-3}/Hz^{1/2}$. With the measured path length (1350 m) and absorption coefficient (1.7×10^{-3}/ppm-m), the noise-equivalent detection limit for ethane is 0.48 ppb /$Hz^{1/2}$. This value was higher than the detector noise limit predicted in the preceding. The extra noise appeared to come from incomplete suppression of the on-axis resonances in the cavity.[85] Exhaled ethane measurements should become more reliable and sensitive with the recent advances[43,44] of TEC CW-DFB ICLs.

4.6.2 *Acetone*

Laser absorption spectroscopy can provide real-time, sensitive, and selective concentration measurements of acetone, which has an absorption band at ~8.0 μm. This absorption band is ~250 times stronger than in near-IR, which facilitates sensor architecture. A Daylight Solutions available mid-IR EC QCL provided a maximum power of 10 mW, and was tunable from 1196 to 1300 cm^{-1}. A strong absorption band results in a 0.1% absorption for a 1-m sampling cell filled with atmospheric pressure air, contaminated by 1 ppm of acetone vapor. This absorption was detected by traditional absorption spectroscopy using a pyroelectric detector. Wavelength modulation spectroscopy improves the detection limit up to 10 times and results in a 100 ppbv detection sensitivity.[86]

5 Summary and Breath Requirements for the Future

Compact, sensitive, and selective chemical sensors based on QCLs were demonstrated to be effective in clinical studies that involved the detection and monitoring of large number of exhaled biomarkers (e.g., NO, CO, CO_2, NH_3, C_2H_6, and COS) using LAS, cavity-enhanced spectroscopy, FRS, PAS, and QEPAS sensing architectures. With the ongoing development of efficient mid-IR lasers[87–92] we envision a significant reduction of the size and cost of QCL trace gas monitors that will lead to the availability of commercial breath analyzers and wearable, ultracompact sensors.[93]

Although clinical breath analysis is currently in its infancy, it offers unique capabilities to the field of medicine. Breath can be collected multiple times from humans without posing any risk to the subject or the person collecting the sample. Real-time monitors are currently being developed and these devices could be well suited for field and epidemiological studies, particularly for studies in developing countries where collecting blood and urine samples are difficult without refrigeration. If inexpensive, portable, real-time monitors can be developed, then chronically sick patients could monitor their progress in their home and thereby minimize their exposure to infections during routine visits to clinics. Breath analysis can be used to detect disease, monitor disease progression, or monitor therapy. Breath analysis can be used for phase 1 and phase 2 clinical trials to monitor new drug therapy or to detect potential adverse effects. Since breath analysis is noninvasive and can be performed easily, it allows larger numbers of subjects to be studied. If larger numbers of human subjects are studied, unusual adverse effects of new pharmacologic agents are more likely to be identified earlier.

Acknowledgments

Financial support of the research was provided by the National Science Foundation via a subaward from the Princeton University Mid-InfraRed Technologies for Health and the Environment (MIRTHE) Engineering Research Center (ERC), the National Aeronautics and Space Administration via awards from the Jet Propulsion Laboratory, Pasadena, California, and the Johnson Space Center, Houston, Texas, and Grant No. C-0586 from the Robert Welch Foundation.

References

1. L. Pauling, A. B. Robinson, R. Teranishi, and P. Cary, "Quantitative analysis of urine vapor and breath by gas-liquid partition chromatography," *Proc. Natl. Acad. Sci.* **68**, 2374–2376 (1971).
2. S. Chen, L. Zieve, and V. Mahadevan, "Mercaptans and dimethyl sulfide in the breath of patients with cirrhosis of the liver. Effect of feeding methionine," *J. Lab. Clin. Med.* **75**, 628–635 (1970).
3. C. A. Riely, G. Cohen, and M. Lieberman, "Ethane evolution: a new index of lipid peroxidation," *Science* **183**, 208–210 (1974).
4. J. R. Dannecker, E. G. Shaskan, and M. Phillips, "A new highly sensitive assay for breath acetaldehyde: detection of endogenous levels in humans," *Anal. Biochem.* **114**, 1–7 (1981).

5. A. S. Modak, "Stable isotope breath tests in clinical medicine: a review," *J. Breath. Res.* **1**, 014003 (2007).
6. B. O. Jansson and B. T. Larsson, "Analysis of organic compounds in human breath by gas chromatography-mass spectrometry," *J. Lab. Clin. Med.* **74**, 961–966 (1969).
7. E. S. Deneris, R. A. Stein, and J. F. Mead, "In vitro biosynthesis of isoprene from mevalonate utilizing a rat liver cytosolic fraction," *Biochem. Biophys. Res. Commun.* **123**, 691–696 (1984).
8. B. G. Stone, T. J. Besse, W. C. Duane, C. D. Evans, and E. G. DeMaster, "Effects of regulating cholesterol biosynthesis on breath isoprene excretion in men," *Lipids* **28**, 705–708 (1993).
9. T. H. Risby, "Volatile organic compounds as markers in normal and diseased states," in *Disease Markers in Exhaled Breath: Basic Mechanisms and Clinical Applications*," N. Marczin, and M. Yacoub, Eds., pp. 113–122, NATO ASI Series, IOS Press, Amsterdam (2002).
10. T. H. Risby and S. S. Sehnert, "Clinical application of breath biomarkers of oxidative stress status," *Free Rad. Biol. Med.* **27**, 1182–1192 (1999).
11. L. E. Otterbein, D. Morse, A. Choi, and J. T. Chapman, "Carbon monoxide a gaseous molecule with anti-inflammatory properties," in *Disease Markers in Exhaled Breath*, N. Marczin, S. Kharitonov, M. Yacoub, and P. Barnes, Eds. pp. 133–156, Marcel Dekker, London (2002).
12. D. K. Stevenson and H. J. Vreman, "Carbon monoxide and bilirubin production in neonates," *Pediatrics* **100**, 252–259 (1997).
13. ~~C. N. Tassopoulos,~~ D. Barnett, and T. R. Fraser, "Breath acetone and blood sugar measurements in diabetes," *Clin. Sci.* **37**, 570 (1969). Q2
14. P. L. Davis, L. A. Dal Cortivo, and J. Maturo, "Endogenous isopropanol: forensic and biochemical implications," *J. Analyt. Toxicol.* **8**, 209–212 (1984).
15. K. Cope, T. Risby, and A. Diehl, "Increased gastrointestinal ethanol production in obese mice: implications for fatty liver disease pathogenesis," *Gasteroenterology* **119**, 1340–1347 (2000).
16. W. F. Borson and T. K. Li, "Genetic polymorphism of human liver alcohol and aldehyde dehydrogenases and their relationships to alcohol metabolism," *Hepatology* **6**, 502–510 (1994).
17. J. Axelrod and J. Daly, "Pituitary gland: enzymic formation of methanol from S-adenosylmethionine," *Science* **150**, 892–893 (1965).
18. S. Moncada, "Nitric oxide gas: mediator, modular and pathophysiologic entity," *Lab. Clin. Med.* **120**, 187–191 (1992).
19. L. E. Gustafsson, A. M. Leone, M. G. Persson, N. P. Wiklund, and S. Moncada, "Endogenous nitric oxide is present in the exhaled air of rabbits, guinea pigs, and humans," *Biochem. Biophys. Res. Commun.* **181**, 852–857 (1991).
20. S. Kharitonov, K. Alving, and P. J. Barnes, "Exhaled and nasal nitric oxide measurements: recommendations," *Eur. Respir. J.* **10**, 1683–1693 (1997).
21. "American Thoracic Society Recommendations for standardized procedures for the online and offline measurement of exhaled lower respiratory nitric oxide and nasal nitric oxide in adults and children," *Am. J. Respir. Crit. Care Med.* **160**, 2104–2117 (1999).
22. ATS/ERS, "Recommendations for standardized procedures for the online and offline measurement of exhaled lower respiratory nitric oxide and nasal nitric oxide," *Am. J. Respir. Crit. Care Med.* **171**, 912–1930 (2005).
23. M. L. Simenhoff, J. F. Burke, J. J. Saukkonen, A. T. Ordinario, and R. Doty, "Biochemical profile of uremic breath," *New Engl. J. Med.* **297**, 132–135 (1977).
24. S. Davies, P. Spanel, and D. Smith, "Quantitative analysis of ammonia on the breath of patients in end-stage renal failure," *Kidney Int.* **52**, 223–228 (1997).
25. K. A. Cope, "Breath biomarkers of exposure and disease," PhD Dissertation, Johns Hopkins University (2002).
26. S. F. Solga and T. H. Risby, "What is normal breath? challenge and opportunity," *IEEE Sens. J.* **10**, 7–9 (2010).
27. T. H. Risby and S. F. Solga, "Current status of clinical breath analysis," *Appl. Phys. B* **85**, 421–426 (2006).
28. R. F. Curl, F. Capasso, C. Gmachl, A. A. Kosterev, B. McManus, R. Lewicki, M. Pusharsky, G. Wysocki, and F. K. Tittel "Quantum cascade lasers in chemical physics," *Chem. Phys. Lett. Front. Art.* **487**, 1–18 (2010).
29. J. H. Shorter, D. D. Nelson, J. B. McManus, M. S. Zahniser, and D. K. Milton, "Multicomponent breath analysis with infrared absorption using room-temperature quantum cascade lasers," *IEEE Sens. J.* **10**, 76–84 (2010).
30. S. Kim, C. Young, B. Vidakovic, S. G. A. Gabram-Mendola, C. W. Bayer, and B. Mizaikoff, "Potential and challenges for mid-infrared sensors in breath diagnostics," *IEEE Sens. J.* **10**, 145–158 (2010).
31. A. A Kosterev and F. K. Tittel, "Chemical sensors based on quantum cascade lasers," *IEEE J. Quantum Electron.* **38**, 582–591 (2002).
32. M. J. Thorpe, D. Balslev-Clausen, M. S. Kirchner, and J. Ye, "Cavity-enhanced optical frequency comb spectroscopy: application to human breath analysis," *Opt. Express* **16**, 2387–3297 (2008).
33. A. A. Kosterev, A. L. Malinovsky, F. K. Tittel, C. Gmachl, F. Capasso, D. L. Sivco, J. N. Baillargeon, A. L. Hutchinson, and A. Y. Cho, "Cavity ring-down spectroscopy of NO with a single frequency quantum cascade laser," *Appl. Opt.* **40**, 5522–5529 (2001).
34. Y. A. Bakhirkin, A. A. Kosterev, R. F. Curl, F. K. Tittel, D. A. Yarekha, L. Hvozdara, M. Giovannini, and J. Faist, "Sub-ppbv nitric oxide concentration measurements using cw room-temperature quantum cascade laser based integrated cavity spectroscopy," *Appl. Phys. B* **82**, 149–154 (2006).
35. A. A. Kosterev, Y. A. Bakhirkin, and F. K. Tittel, "Ultrasensitive gas detection by quartz-enhanced photoacoustic spectroscopy in the fundamental molecular absorption bands region," *Appl. Phys. B* **80**, 133–138 (2005).
36. J. Faist, D. Hofstetter, M. Beck, T. Aellen, M. Rochat, and S. Blaser, "Bound-to-continuum and two-phonon resonance quantum-cascade lasers for high duty cycle, high-temperature operation," *IEE J. Quantum Electron.* **38**, 533–546 (2002).
37. C. Gmachl, D. L. Sivco, R. Colombelli, F. Capasso, and A. Y. Cho, "Ultra-broadband semiconductor laser," *Nature* **415**, 883–887 (2002).
38. R. Maulini, A. Mohan, M. Giovannini, J. Faist, and E. Gini, "External cavity quantum-cascade lasers tunable from 8.2 to 10.4 um using a gain element with a heterogeneous cascade," *Appl. Phys. Lett.* **88**, 201113 (2006).
39. ~~R. Maulini, M. Beck, J. Faist, and E. Gini, "Broadband tuning of external cavity bound-to-continuum quantum-cascade lasers," *Appl. Phys. Lett.* **84**, 1659 (2004).~~ Q3
40. C. Peng, G. Luo, and H. Q. Le, "Broadband, continuous and fine-tune properties of external-cavity thermoelectric-stabilized mid-infrared quantum-cascade lasers," *Appl. Opt.* **42**, 4877–4882 (2003).
41. G. Wysocki, R. F. Curl, F. K. Tittel, R. Maulini, J. M. Bulliard, and J. Faist, "Widely tunable mode-hop free external cavity quantum cascade laser for high resolution spectroscopic applications," *Appl. Phys. B* **81**, 769–777 (2005).
42. A. Kosterev, G. Wysocki, Y. Bakhirkin, S. So, R. Lewicki, F. Tittel, and R. F. Curl, "Application of quantum cascade lasers to trace gas analysis," in "Selected papers from the International Conference on Tunable Lasers and Fundamental Laser Spectroscopy," M. Sigrist, Ed., *Appl. Phys. B* **90**, 165–176 (2008).
43. C. S. Kim, M. Kim, W. W. Bewley, J. R. Lindle, C. L. Canedy, J. Abell, I. Vurgaftman, and J. R. Meyer, "Corrugated-sidewall interband cascade lasers with single-mode midwave-infrared emission at room temperature," *Appl. Phys. Lett.* **95**, 231103 (2009).
44. I. Vurgaftman, C. L. Canedy, C. S. Kim, M. Kim, W. W. Bewley, J. R. Lindle, J. Abell, and J. R. Meyer, "Mid-infrared interband cascade lasers operating at ambient temperatures," *New J. Phys.* **11**, 125015 (2009).
45. M. Kim, C. L. Canedy, C. S. Kim, W. W. Bewley, J. R. Lindle, J. Abell, I. Vurgaftman, and J. R. Meyer, "Room temperature interband cascade lasers," *Phys. Proc.* **3**, 1195–1200 (2010).
46. J. U. White, "Long optical paths of large aperture," *J. Opt. Soc. Am.* **32**, 285–288 (1942).
47. D. R. Herriott and H. J. Schulte, "Folded optical delay lines," *Appl. Opt.* **4**, 883–889 (1965).
48. J. B. McManus, P. L. Kebabian, and M. Zahniser, "Astigmatic mirror multipass absorption cells for long-path-length spectroscopy," *Appl. Opt.* **34**, 3336–3348 (1995).
49. A. O'Keefe and D. A. G. Deacon, "Cavity ring-down optical spectrometer for absorption measure using pulsed laser sources," *Rev. Sci. Instrum.* **59**, 2544 (1988). Q4
50. J. J. Scherer, J. B. Paul, A. O'Keefe, and R. J. Saykally, "Cavity ring-down laser absorption spectroscopy: history, development, and application to pulsed molecular beams," *Chem. Rev.* **97**, 25–52 (1997).
51. M. Mazurenka, A. J. Orr-Ewing, R. Peverall, and G. A. D. Ritchie, "Cavity ring-down and cavity enhanced spectroscopy using diode lasers," *Ann. Rep. Pro. Chem. Sect. C Phys. Chem.* **101**, 100–142 (2005).
52. J. Manne, O. Sukhorukuv, W. Jaeger, and J. Tulip, "Pulsed quantum cascade laser-based cavity ring-down spectroscopy for ammonia detection in breath," *Appl. Opt.* **45**, 9230–9237 (2006).
53. B. A. Paldus, C. C. Harb, T. G. Spence, R. N. Zare, C. Gmachl, F. Capasso, D. L. Sivco, J. N. Baillargeon, A. L. Hutchinson, and A. Y. Cho, "Cavity ringdown spectroscopy using mid-infrared quantum-cascade laser," *Opt. Lett.* **25**, 666–668 (2000).
54. B. A. Paldus, E. R. Crosson, and H. Dahnke, "Practical applications of CRDS in medical diagnostics," Chap. 15 in *Laser in Environmental and Life Sciences: Modern Analytical Methods*, P. Hering, J. P. Lay, and S. Stry, Eds., pp. 297–311, Springer-Verlag, Berlin (2004).
55. H. Dahnke, S. Stry, and G. Basum "Medical trace gas detection by means of mid-infrared cavity leak-out spectroscopy," Chap. 14 in *Laser in Environmental and Life Sciences: Modern Analytical Methods*, P. Hering, J. P. Lay, and S. Stry, Eds. pp. 283–295, Springer-Verlag, Berlin (2004).
56. G. S. Engel, W. S Drisdell, F. N. Keutsch, E. J. Moyer, and J. G. Anderson, "Ultrasensitive near-infrared integrated cavity output spectroscopy technique for detection of CO at 1.57 μm: new sensitivity limits for absorption measurements in passive optical cavities," *Appl. Opt.* **45**, 9221–9229 (2006).
57. A. O'Keefe, J. J. Scherrer, and J. B. Paul, "Integrated cavity output analysis of ultraweak absorption," *Chem. Phys. Lett.* **307**, 343–349 (1999).
58. J. B. Paul, L. Lapson, and J. G. Anderson, "Ultrasensitive absorption

spectroscopy with a high-finesse optical cavity and off-axis alignment," *Appl. Opt.* **40**, 4904–4910 (2001).
59. M. R. McCurdy, Y. Bakhirkin, G. Wysocki, and F. K. Tittel, "Performance of an exhaled nitric oxide and carbon dioxide sensor using quantum cascade laser based integrated cavity output spectroscopy," *J. Biomed. Opt.* **12**, 34034 (2007).
60. A. A. Kosterev, Y. A. Bakhirkin, R. F. Curl, and F. K. Tittel, "Quartz-enhanced photoacoustic spectroscopy," *Opt. Lett.* **27**, 1902–1904 (2002).
61. A. A. Kosterev, F. K. Tittel, D. Serebryakov, A. Malinovsky, and A. Morozov, "Applications of quartz tuning fork in spectroscopic gas sensing," *Rev. Sci. Instrum.* **76**, 043105 (2005).
62. A. A. Kosterev and F. K. Tittel, "Ammonia detection by use of quartz-enhanced photoacoustic spectroscopy with a near-IR telecommunication diode laser," *Appl. Opt.* **43**, 6213–6217 (2004).
63. G. Wysocki, A. A. Kosterev, and F. K. Tittel, "Influence of molecular relaxation dynamics on quartz-enhanced photoacoustic detection of CO_2 at $\lambda = 2\ \mu$m," *Appl. Phys. B* **85**, 301–306 (2006).
64. D. Weidmann, A. A. Kosterev, F. K. Tittel, N. Ryan, and D. McDonald, "Application of widely electrically tunable diode laser to chemical gas sensing with quartz-enhanced photoacoustic spectroscopy," *Opt. Lett.* **29**, 1837–1839 (2004).
65. A. A. Kosterev, Y. A. Bakhirkin, and F. K. Tittel, "Ultrasensitive gas detection by quartz-enhanced photoacoustic spectroscopy in the fundamental molecular absorption bands region," *Appl. Phys. B* **80**, 133–138 (2005).
66. C. Roller, A. A. Kosterev, F. K. Tittel, K. Uehara, C. Gmachl, and D. L. Sivco, "Carbonyl sulfide detection with a thermoelectrically cooled mid-infrared quantum cascade laser," *Opt. Lett.* **28**, 2052–2054 (2003).
67. G. Wysocki, M. McCurdy, S. So, D. Weidmann, C. Roller, R. F. Curl, and F. K. Tittel, "Pulsed quantum cascade laser based sensor for trace-gas detection of carbonyl sulfide," *Appl. Opt.* **43**, 6040–6046 (2004).
68. A. A. Kosterev, T. S. Mosely, and F. K. Tittel, "Impact of humidity on quartz enhanced photoacoustic spectroscopy based detection of HCN," *Appl. Phys. B* **85**, 295–300 (2006).
69. M. Horstjann, Y. A. Bakhirkin, A. A. Kosterev, R. F. Curl, and F. K. Tittel, "Formaldehyde sensor using interband cascade laser based quartz-enhanced photoacoustic spectroscopy," *Appl. Phys. B* **79**, 799–803 (2004).
70. H. Miller, Y. A. Bakhirkin, T. Ajtai, and F. K. Tittel, C. J. Hill, and R. Q. Yang "Detection of formaldehyde using off-axis integrated cavity output spectroscopy with an interband cascade laser," *Appl. Phys. B* **85**, 391–396 (2006).
71. A. Kosterev, F. K. Tittel, T. S. Knittel, A. Cowie, and J. D. Tate, "Trace humidity sensor based on quartz-enhanced photoacoustic spectroscopy," in *Laser Application to Chemical Security and Environmental Analysis (LACSEA 2006), Technical Digest*, Optical Society of America (2006). Q5
72. M. D. Wojcik, M. C. Phillips, B. D. Cannon, and M. S. Taubman, "Gas-phase photoacoustic sensor at 8.41 μm using quartz tuning forks and amplitude-modulated quantum cascade lasers," *Appl. Phys. B* **85**, 307–313 (2006).
73. R. Lewicki, G. Wysocki, A. Kosterev, and F. K. Tittel, "Quartz enhanced photoacoustic spectroscopy based detection of broadband absorbing molecules using a widely tunable, cw mid-infrared quantum cascade laser at 8.4 μm," *Opt. Express* **15**, 7357–7366 (2007).
74. M. R. McCurdy, Y. A. Bakhirkin, and F. K. Tittel, "Quantum cascade laser-based integrated cavity output spectroscopy of exhaled nitric oxide," *Appl. Phys. B* **85**, 445–452 (2006).
75. K. Namjou, C. B. Roller, T. E. Reich1, J. D. Jeffers, G. L. McMillen, P. J. McCann, and M. A. Camp, "Determination of exhaled nitric oxide distributions in a diverse sample population using tunable diode laser absorption spectroscopy," *Appl. Phys. B* **85**, 427–435 (2006).
76. P. W. Werle, "Diode-Laser Sensors for In-Situ Gas Analysis," Chap. 11 in *Laser in Environmental and Life Sciences: Modern Analytical Methods*, P. Hering, J. P. Lay, and S. Stry, pp. 223–243, Springer-Verlag, Berlin (2004).
77. M. McCurdy, Y. Bakhirkin, G. Wysocki and F. K Tittel, "Recent advances of laser spectroscopy based techniques for applications in breath analysis," *J. Breath Res.* **1**, 014001 (2007).
78. R. Lewicki, J. H. Doty, R. F. Curl, F. K. Tittel, and G. Wysocki, "Ultrasensitive detection of nitric oxide at 5.33 μm using external cavity quantum cascade laser based faraday rotation spectroscopy," *Proc. Natl. Acad. Sci. U.S.A.* **106**, 12587 (2009).
79. G. Litfin, C. R. Pollock, R. F. Curl, and F. K. Tittel, "Sensitivity enhancement of laser absorption spectroscopy by magnetic rotation effect," *J. Chem Phys.* **72**, 6602 (1980). Q6
80. H. Adams, D. Reinert, P. Kalkert, and W. Urban, "A differential detection scheme for Faraday rotation spectroscopy with a color center laser," *Appl. Phys. B* **34**, 179 (1984).
81. H. Ganser W. Urban, and A. M. Brown, "The sensitive detection of NO by Faraday modulation spectroscopy with a quantum cascade laser," *Mol. Phys.* **101**, 545 (2003).
82. W. Herrmann, W. Rohrbeck, and W. Urban, "Line shape analysis for Zeeman modulation spectroscopy," *Appl. Phys. A* **22**, 71 (1980).
83. W. Urban, "Free radical spectroscopy, a challenge for sensitive detection," Chap. 16 in *Laser in Environmental and Life Sciences: Modern Analytical Methods*, P. Hering, J. P. Lay, and S. Stry, Eds., pp. 269–282, Springer-Verlag, Berlin (2004).
84. S. S. Sehnert, L. Jiang, J. F. Burdick, and T. H. Risby, "Breath biomarkers for detection of human liver diseases: a preliminary study," *Biomarkers* **7**, 174–187 (2002).
85. S. M. Studer, I. Rosa, K. A. Cope, J. Krishnan, J. B. Orens, and T. H. Risby, "Patterns and significance of exhaled breath biomarkers in lung transplant recipients with acute allograft rejection," *J. Heart Lung Transpl.* **20**, 1158–1166 (2001).
86. K. R. Parameswaran, D. I. Rosen, M. G. Allen, A. M. Ganz, and T. H. Risby, "Off-axiz integrated cavity output spectroscopy with a mid-infrared interband cascade laser for real-time breath ethane measurements," *Appl. Opt.* **48**, 73–79 (2009).
87. Y. Bakhirkin, A. A. Kosterev, T. Day, M. Pushkarsky, and F. K Tittel, "Tunable mid-IR external cavity quantum cascade laser based spectroscopic sensor for acetone detection," Presented at SPIE Optics East, Sep. 9–12, 2007, Boston, MA. Q7
88. A. Tsekoun, R. Go, M. Pushkarsky, M. Razeghi, and C. K. N. Patel, "Improved performance of quantum cascade lasers through a scalable, manufacturable epitaxial-side-down mounting process," *Proc. Natl. Acad. Sci. U.S.A* **103**, 4831–4835 (2006).
89. A. Wittmann, M. Giovannini, J. Faist, L. Hvozdara, S. Blaser, D. Hofstetter, and E. Gini, "Room temperature, continuous wave operation of distributed feedback quantum cascade lasers with widely spaced operation frequencies," *Appl Phys. Lett.* **89**, 141116 (2006).
90. J. Faist, "Wallplug efficiency of quantum cascade lasers: Critical parameters and fundamental limits," *Appl. Phys. Lett.* **90**, 253512 (2007).
91. M. Razeghi, "High-performance InP-Based Mid-IR quantum cascade lasers," *IEEE J. Select. Top. Quantum Electron.* **15**, 941–951 (2009).
92. S. Slivken, Y. Bai, B. Gokden, S. R. Darvish, and M. Rhazhegi, "Current status and potential of high power mid-infrared intersubband lasers," *Quantum Sensing and Nanophotonic Devices VII*, edited by M. Rhazhegi. 7608, 76080B (2010).
93. Y. Bai, S. Slivken, S.R. Darvish, and M. Razeghi, "Very high wall plug efficiency of quantum cascade lasers," in *Quantum Sensing and Nanophotonic Devices VII*, M. Rhazhegi, Ed., *Proc. SPIE* **7608**, 76080F (2010).
94. S. So, F. Koushanfar, A. Kosterev, and F. Tittel, "Laser SPECks: laser SPECtroscopic trace gas sensor networks—sensor integration and applications," *Proc. Information Processing in Sensor Networks* (IPSN-SPOTS), Cambridge, MA (2007). Q8 Q9

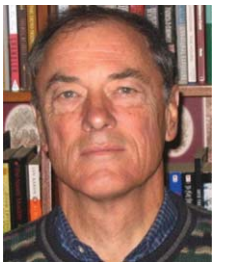

Terence H. Risby is a professor emeritus with the Department of Environmental Health at the Johns Hopkins University Bloomberg School of Public Health. Dr. Risby received his PhD degree in chemistry from Imperial College of Science, Technology and Medicine, London, in 1970. After postdoctoral fellowships at the University of Madrid and the University of North Carolina he became an assistant professor of chemistry at the Pennsylvania State University. In 1979 he became an associate professor of environmental health sciences at Johns Hopkins University and was promoted to professor in 1987. When he retired December 31, 2003, he was a professor of toxicological sciences, professor of pathology, and professor of international health. He was also a member of the Johns Hopkins Center in Urban Environmental Health, the Johns Hopkins Center for Human Nutrition, and the Division of Clinical Chemistry in the Johns Hopkins Hospital.

Frank K. Tittel graduated in 1955 with a BA degree in physics from the University of Oxford, where he received his MA and PhD degrees in physics in 1959. Since 1967 he has been on the faculty of the Department of Electrical and Computer Engineering, Rice University, Houston, Texas, where he is currently the Josephine S. Abercrombie Professor of Electrical and Computer Engineering and holds a joint faculty appointment in the Department of Bioengineering. From 1959 to 1967 he was a research physicist with General Electric Research and Development Center, Schenectady, New York. His current research interests include various aspects of quantum electronics, in particular laser spectroscopy and laser applications in medicine, environmental monitoring, and industrial process control. He is the author and coauthor of more than 350 technical papers in peer-reviewed journals.

Queries

Q1: Au: Pls. check linking for Refs. 2, 6, 13, 14, 18, 21, 28, 42, 59, 79, 82, 86, 89, 93.
Q2: Au: All on one page or please add last for Ref. 13.
Q3: Au: All on one page or please add last for Ref. 39.
Q4: Au: All on one page or please add last for Ref. 49.
Q5: Au: Edit ok per Net Search? Can add pages for Ref. 71?
Q6: Au: All on one page or please add last for Refs. 79–82.
Q7: Au: Au: Inserted “Presented” here, pls. verify this.
Q8: Au: Please cite in order in text.
Q9: Au: Please add pages and publisher/sponsor for Ref. 94.